

Thermal cracking experiment in a salt mine.

Grégoire Hévin, STORENGY,
Cyrille Balland, INERIS,
J. Billiotte, B. Tessier, F. Hadj Hassen, A. Rouabhi, L. Blanco-Martin, MINES PARISTECH/ARMINES,
Kurt Staudtmeister, Bastian Leuger, Dirk Zapf, IUB/Leibniz Universität Hannover,
Emmanuel Hertz, Daniel Tribout, Nicolas Thelier, CSME/Salins.

1 Introduction

Towards the end of the 2000s, the global energy situation began to change significantly. The need for energy transition became increasingly important, pushing players in the field to look into different subjects relating to energy production and use. The energy storage sector was no exception, and research projects into compressed air or hydrogen storage in salt caverns came into being. Within these projects, storage often involves high injection and withdrawal flow rates. This means that pressure (and temperature) variations at the cavern walls take place very quickly and "injection-withdrawal" operating cycles are very frequent.

At the same time, natural gas storage in salt caverns is also faced with demands for ever-faster operation. The traditional operating method known as "seasonal modulation" with a yearly cycle (withdrawal in winter and re-injection in the spring and/or beginning of summer) is brought into question. Demands for monthly or even weekly cycles (withdrawal in the week, re-injection at the week-end) are emerging. These cycles, which are a lot more rapid, generate high temperature variations through the Joule-Thomson effect, and leave little time for heat exchange between the rock and the stored gas. Compared to traditional yearly cycles, the smoothing effect of the temperature variations by heat exchange is a lot more limited.

In this context, the question of the impact of temperature on salt cavern stability especially needs to be raised. To answer it, numerous research projects have been carried out based on digital simulations (Bauer S., 2009; Minkley et al, 2011; Brouard et al, 2011; Pellizzaro et al, 2011, Zapf et al, 2012; Bérest et al, 2012). The theory and models show that if we take temperature into account in the calculations, in some cases, a tensile zone can appear at the cavern wall. As salt tensile strength is relatively low (1 to 2 MPa), this tensile zone could cause cracks at the cavern wall. Note that this tensile zone is not deep from the wall (skin effect at structure scale) and does not affect the overall stability of the structure the consequences of the potential cracking and its limits should be assessed. However, the results of these studies come up against the lack of experimental data for confirming the calculations, the effects being too fine to be observed in actual conditions.

In 2012, the Solution Mining Research Institute (SMRI) launched a Request For Proposals for an experiment that would make it possible to further understanding of the actual impacts of temperature variations on a salt wall, and to validate the theoretical approaches. To be able to produce significant results, the SMRI compiled specific specifications including twelve recommendations:

1. since a larger salt wall surface is more favourable for the development of fractures, the minimum cooled salt wall surface area should be 10 m²;
2. the cooling of the salt wall should be performed by using a gas (air, nitrogen, etc.), and it should be sufficient to initiate fractures, taking into consideration the pre-existing stress state at the salt wall;

3. a cooling phase should last several weeks, long enough time to ensure that the temperature changes extend to appropriate depth into the salt wall;
4. several successive phases of cooling should be applied, so that the effect of repeated temperature cycles can be examined;
5. applying gas pressure to the salt wall, in addition to the cooling, would be more representative of the real situation in a gas storage cavern, but using gas pressure for such a test may not be practical, due to mine safety / security requirements.
6. the test must be conceived in such a way that the fractures are visible, and that their progression/propagation can be observed, measured and photographed;
7. Instrumentation must make temperature measurements in the gas, at the salt wall, and at various depths in the salt, so that temperature distribution and changes are recorded and analysed.
8. when a fracture appears, measurements should document crack growth over time;
9. acoustic emission measurements are required;
10. after the test, the salt wall should be cored, in such a way that the penetration of the fractures in the salt can be measured;
11. thermo-mechanical computations should be performed: before the field experiment to design the test, and after the tests to interpret results;
12. SMRI encourages complementary team approaches and proposals, which will cover more possibilities and result in more thorough analysis, and may lead to an international consensus.

An international team was set up to answer the RFP. It included the Compagnie des Salins du Midi et des Salines de l'Est (CSME - Salins group), the INERIS, Mines ParisTech'/ARMINES, de IUB/Leibniz Universität Hannover and Storengy. The team proposed carrying out a full-scale experiment on a salt slab in an experimental gallery excavated especially in the Varangéville salt mine, near to Nancy.

The planned operation consisted of applying cooling and heating cycles to an area measuring 10m² in the centre of the slab (recommendation 1). To cool the salt, a refrigerating machine is built inside the gallery for producing cold air which is propelled onto the salt surface via the appropriate ventilation system. The pre-existing stresses are removed from the salt slab by vertical cuts at its boundaries (recommendation 2).

Three cooling-heating cycles are implemented with a 20°C temperature drop (from 14°C, initial mine temperature, to -6°C) (recommendation 4). Cooling time was estimated at 28 days at least for cooling to reach the appropriate depth in the salt (recommendation 3). A last cooling cycle at -6°C then -25°C will be used to end the experiment. Given the mechanical unloading of the slab, the tensile stress generated by thermal cooling is only confronted with very low initial compressive stress. This means the experiment can be carried out at atmospheric pressure (recommendation 5).

The entire test is monitored using a highly comprehensive experimental system: temperature sensors, strain gauges, ultrasonic sensors placed on the surface and at depth. A digital and thermal surface imaging system is also set up (recommendations 6, 7, 8 and 9). At the end of the test, the refrigerating machine is dismantled to be able to take core samples in the salt and to assess crack depth (recommendation 10).

From the resulting data, fine analysis of the phenomena, based on thermomechanical digital simulations, is carried out by two independent laboratories (Mines ParisTech' and IUB). These

analysis should confirm various aspects of the experiment for which only a theoretical approach was possible until now (recommendations 11 and 12).

Based on this proposal which precisely met the SMRI's RFP, the team was selected to carry out the project.

This report is a summary of the various steps of this experiment. After this introductory section, the main elements are presented according to the following outline:

- The second section describes the experimental site and the conditions in which it was built.
- The third section sets out the conditions in which the experiment was conducted and describes in detail the actual thermal stresses applied to the salt formation.
- The fourth section presents the observations and results.
- The fifth part presents the two different interpretations of the experiment on the basis of digital models. They can be used to understand the phenomena coming into play and to quantify them.
- The last section includes the conclusions.

This report shows how this unusual experiment demonstrates the impact of temperature on a salt wall. It also provides quantitative elements on the cracking phenomenon related to cooling, which means this phenomenon can potentially be included in salt cavern storage facility design studies.

2 Experimental site

The salt mine of Varangeville is located close to Nancy, in the east of France. The salt mine is at 120 m from the surface. It is located at the base of the third layer of the Keuper salt formation where the global salt content is around 94%. The mine is operated by the room and pillar method : the galleries (rooms) are 13-meter wide, 4.5-meter high, the pillar are 29-meter wide.

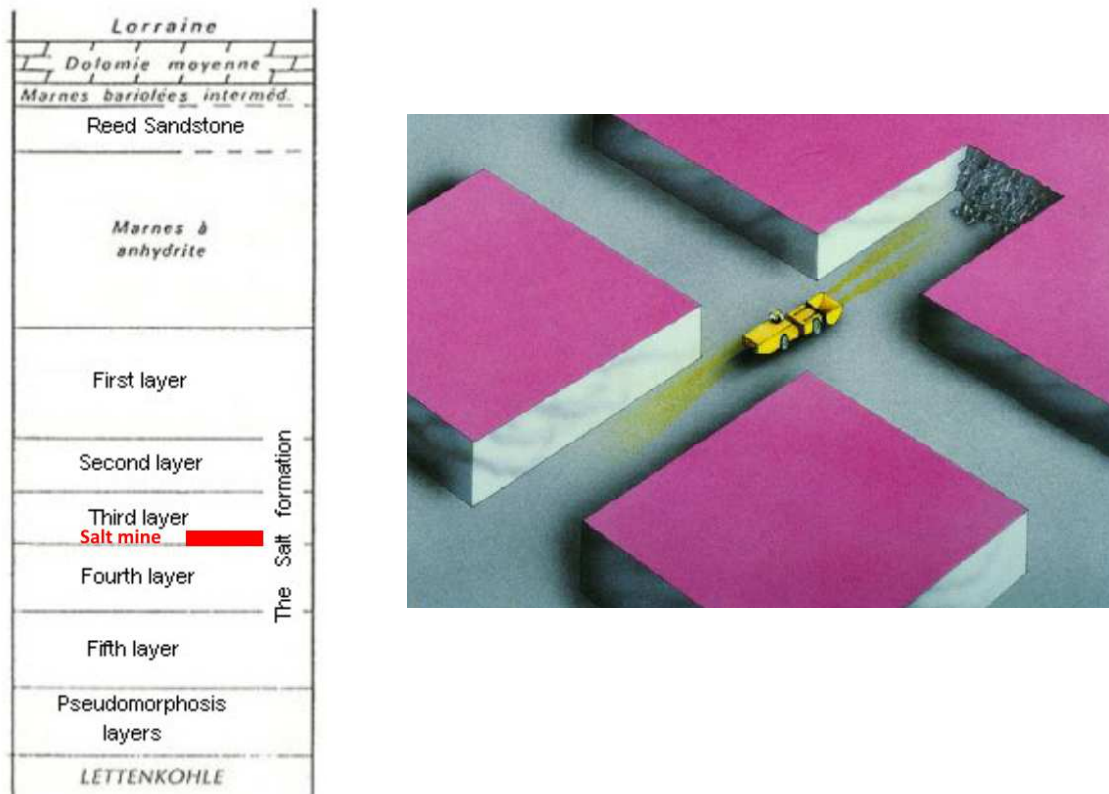


Figure1: Stratigraphic column of Keuper formation in Lorraine salt basin (on the left). 3D view of the room and pillar method and the experimental dead-end gallery (on the right).

To conduct the experiment, a small dead-end gallery was especially excavated. It measures 13 m wide by 18 m long (See Figure2). A salt slab, 1.5 m thick was kept at the floor of the last 12 metres of the gallery. To minimize the influence of *in situ* stresses, two vertical cuts were created along the lateral walls, across the length of the gallery and the entire block thickness. The cuts are 15 cm wide. The cut-out salt block is therefore free on four of the six faces: the upper horizontal face, the front face and the two side faces. The block remains in contact with the formation on its lower face and back face at the back of the gallery where cuts could not be made.

A horizontal surface measuring 3.5 x 3.5 m was created to carry out the experiment. To position it, a surface analysis of the floor of the gallery was carried out to identify eventual cracks caused by blasting or relating to the structural elements of the salt formation. Varangéville salt has desiccation cracks with fossil content. The cracks are vertical and filled with fine vertical layers of clay and salt. To minimize any effect they may have during the experiment, the surface was placed in an even salt zone, away from desiccation cracks. The surface was then prepared for the experiment. It was first flattened then polished.

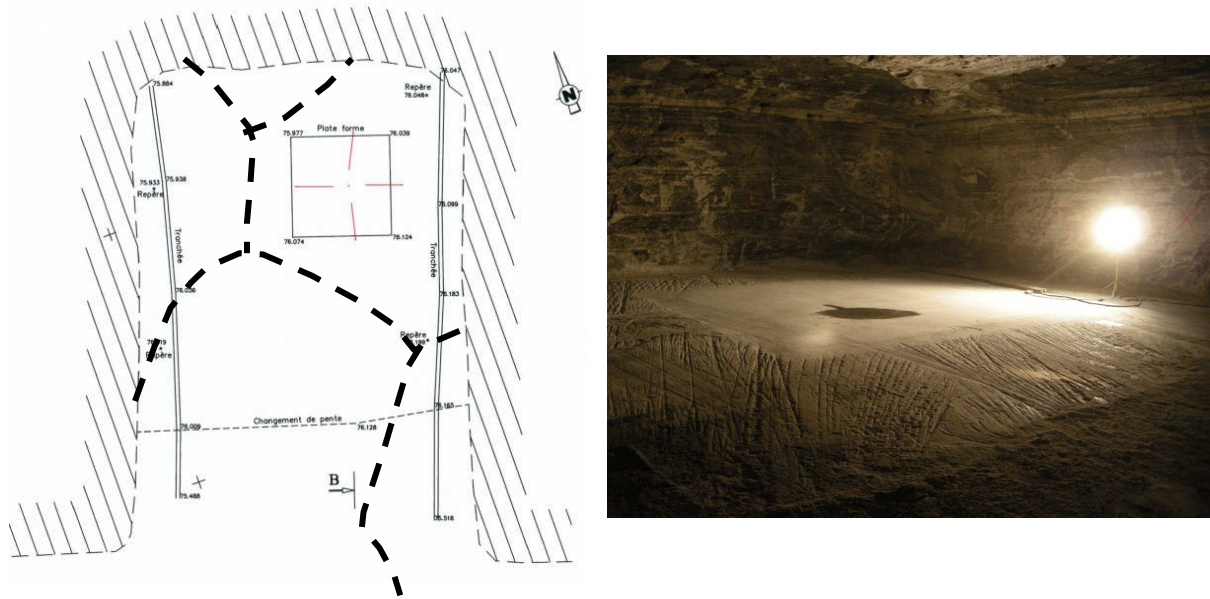


Figure2: Left, plan of the experimental gallery, we note the two cuts to the right and left of the gallery and the desiccation cracks (black dotted lines). The 10m² experimental surface (black rectangle) is placed in an even salt area between the cuts and the desiccation cracks. The red lines show the position of the angled drilling in order to be able to place sensors under the salt surface. Right, photo of the experimental surface after polishing.

A cold room was built on the experimental surface (See Figure3). The refrigerating machine has 5 kW power. The machine was designed to reduce the temperature of the salt from 14.6°C, initial mine temperature to -6°C, therefore a drop of at least 20°C. The design takes account of heating caused by the instrumentation, the presence of observers in the room and heat loss through the walls and through the salt itself, under the room walls.

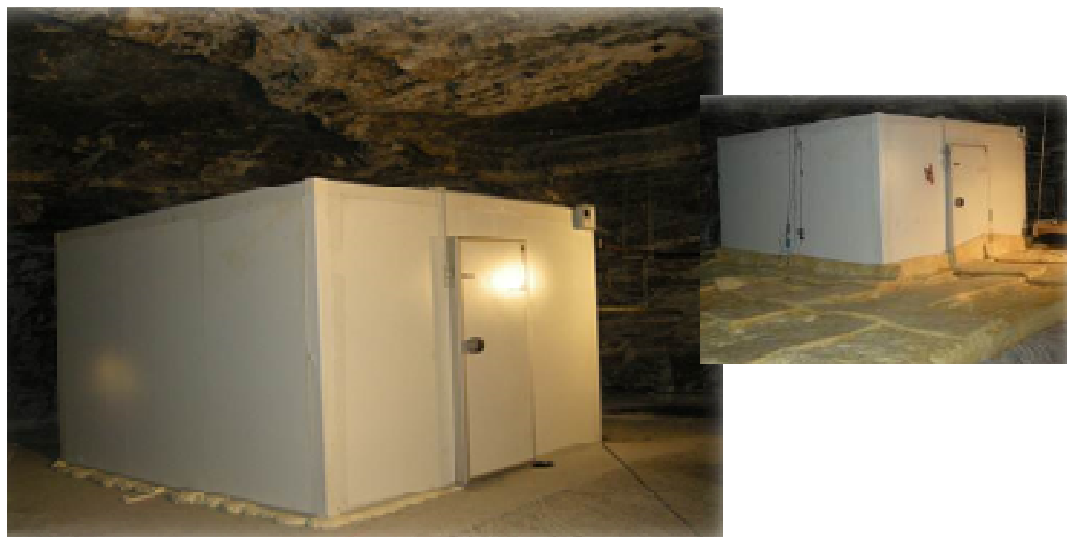


Figure3: Cold room built on the experimental surface and view of the insulation cover surrounding the cold room (on the right).

To minimize heat losses, the floor around the room is covered with heat insulation material during the cooling phase (See Figure3, right). To ensure target temperatures are reached, the power of the refrigerating machine is oversized. An overdesign of the frigorific power is nevertheless taken into account. In theory, the margin allows to potentially reduce the temperature of the salt to -25°C, therefore a more than 35°C difference compared to the initial temperature.

A number of fans placed on the floor of the room ensure a cold air flow in the direction of the ground. Taking account of the heat flux between the air of the room and the salt, an air temperature of -9°C is required to reach a salt temperature of -6°C , which corresponds to the target 20°C difference compared to the initial temperature.

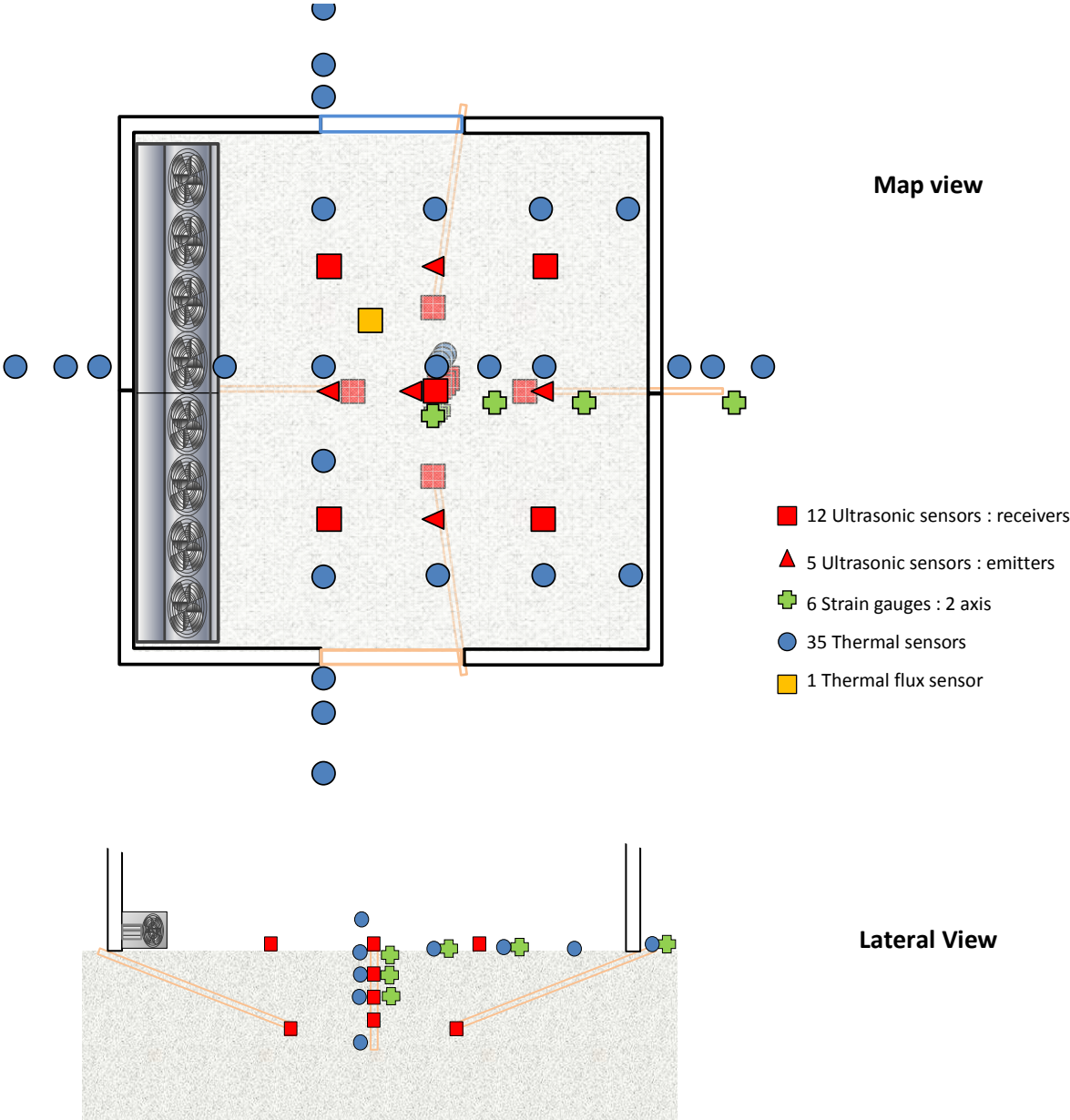


Figure4: Experimental system diagram showing sensor position

5 bore holes were drilled for the instruments: one vertical, 80 cm deep at the centre of the room and 4 angled bore holes from the outside of the room to 60 cm vertical depth for placing the sensor under the room without damaging the surface of it (See Figure4).

35 temperature sensors were set up to monitor the temperature variation between the cooling and heating cycles. They are placed at the surface, inside and outside the room, and also in the central bore hole (up to 80 cm deep). Finally, some sensors are placed above the surface to check the air temperature inside the room. A heat flux sensor is placed on the surface of the floor of the room to measure the flux between the air in the room and the salt.

To measure salt strains, six strain gauges were stuck at the surface in the room and in the central bore hole.

An ultrasonic network was also set up. It comprises 12 receivers and 5 emitters. The receivers are placed in the room on and below the surface (in the central bore hole and in the angled bore holes) for three-dimensional gridding.



Figure5: Left: Picture of the temperature sensors, strain gauges, heat flow sensor and ultrasound sensors on the room surface. To the right, on the room ceiling, the 4 heat-protected digital cameras, thermal camera on its carousel and LED lighting at different places on the door.

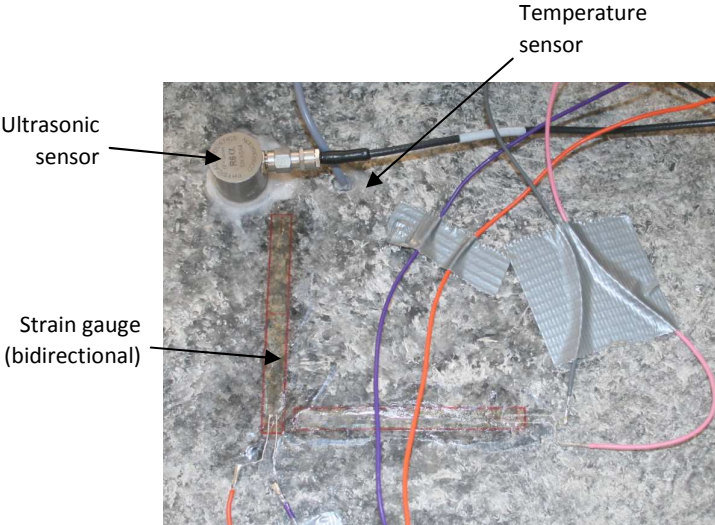


Figure6: Sensors in detail

Finally, an imaging system for viewing any thermal cracking and its spread completed the instrumentation. Four digital cameras attached to the ceiling of the room cover the entire surface area. They are wrapped in heat insulation with a small heater to maintain their temperature above 0°C. They are controlled from outside the room and have 3 pixels per millimetre precision at the salt surface. An infra-red camera is also placed on the room ceiling to view the room surface temperature. To cover the entire surface area with sufficient precision, the IR camera is placed on a rotating system controlled from outside. The imaging system is completed with LED lighting (low heat emitting).

3 Experiment procedure

3.1 Thermal stress

The experiment consists of running 3 cooling-heating cycles. Each cooling and heating phase lasts at least 28 days. Phase length was determined by preparatory thermal calculations taking account of the room's geometry, heat exchange in the walls and heat exchange with outside. As explained previously, room air temperature is reduced by 15°C to -9°C.

During the cooling phase, 28 days are sufficient to reduce the temperature by 20°C over the entire slab thickness (1.5 m). Cooling is monitored on the basis of a strong contrast between the salt surface and depth temperature through to an almost even temperature in the salt.

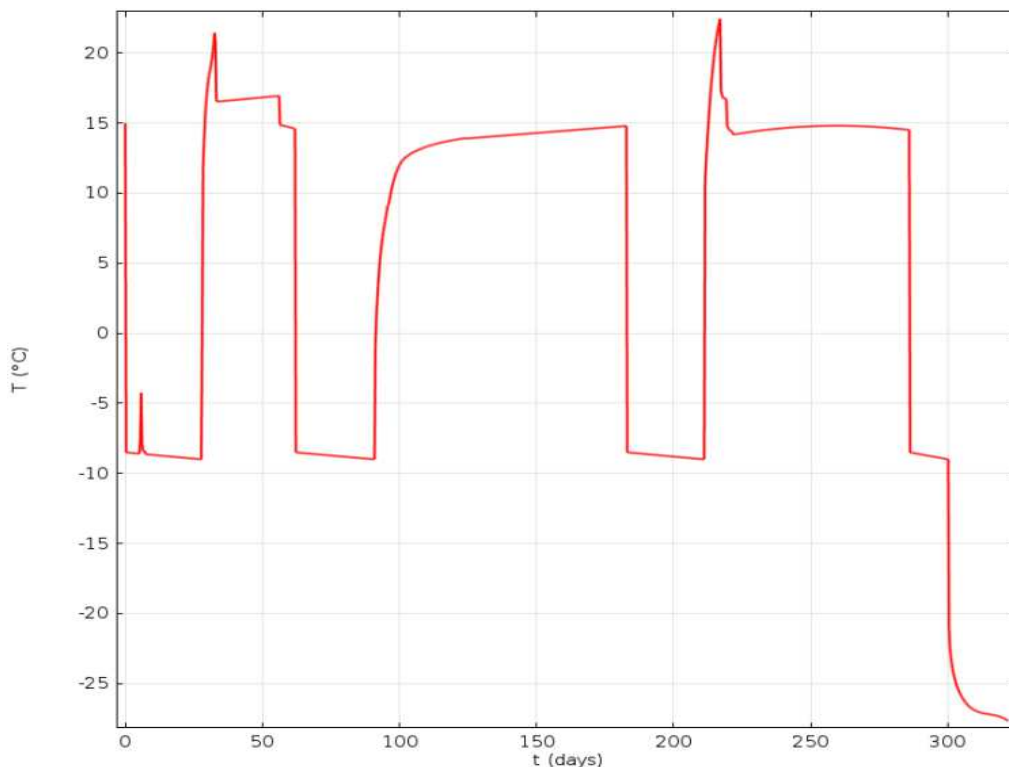


Figure7: Change in cold room air temperature during the experiment. Initial room temperature is 14.6°C.

During the heating phase, 28 days are sufficient, according to the calculations, for returning to almost the initial temperature of the mine. Heating takes place by stopping the refrigerating machine and removing the heat insulation around the room. In practice, the heating phases were slightly longer than the cooling phases (See Figure7). We also note that when heating for the first time, the temperature rose to slightly above the initial 15°C. This is related to the heating strategy: the refrigerating machine was stopped but the doors of the room were kept closed and the fans remained on to force air stirring in the room. The objective was to attempt to heat the system while minimising penetration of moist air in the room and the risk of liquid water condensation at the cold salt surface. This strategy did not prevent condensation however. It especially resulted in the slight temperature excursion due to the heating from fan operation. This strategy was not used when heating for the second time, but was used for the first three days of the 3rd heating phase. In any case, the temperature returned to its initial level at the end of the heating phase.

A fourth cooling cycle took place at the end of the experiment, after the 3 cooling-heating cycles. It consisted of reproducing cooling in the same way as previously over 14 days, before reducing the temperature to -25°C over the next 14 days, this temperature being reached at the refrigerating machine's maximum capacity.

3.2 Surface temperature measurements

The various temperature sensors set up in the room were used to confirm thermal stress in the salt formation.

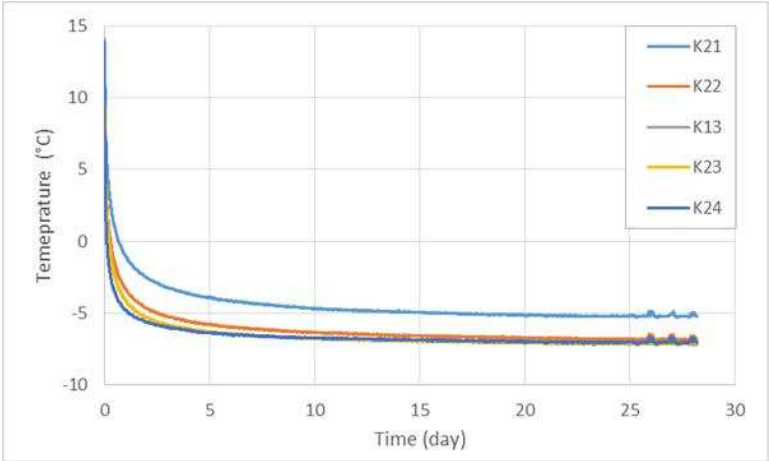


Figure 8: Temperatures as a function of time along the main axial profile

Figure 8 shows the temperature recorded during a cooling cycle, according to an axial profile parallel to the centre of the room. The sensors are placed from K24, closest to the fans, to K21, the farthest from the fans. Temperatures along this main axial are sharply decreasing during the two first days then they slowly trend to a quite constant value. The K21 sensor is placed at the edge of the room, right next to the wall opposite the fans.

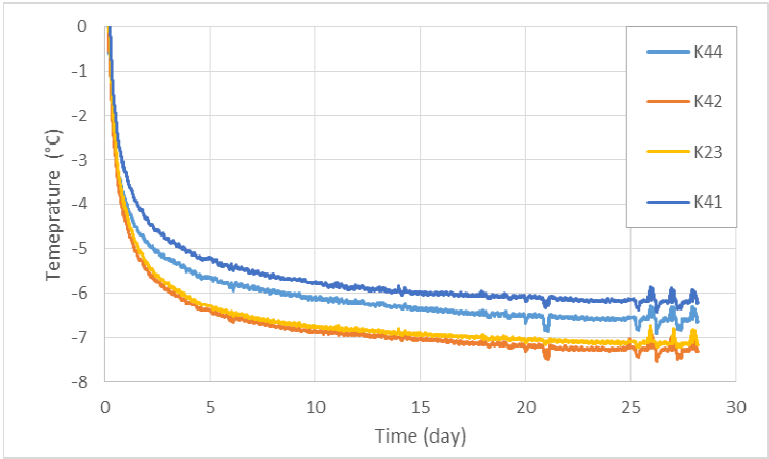


Figure 9 : Temperatures of thermocouples along the main transverse profile

A similar trend is observed on the curves traced according to a transversal profile (Figure 9). The sensors located at the edges, near the room walls (K41 and K44 on Figure 9) show a slightly higher temperature than those nearer the centre.

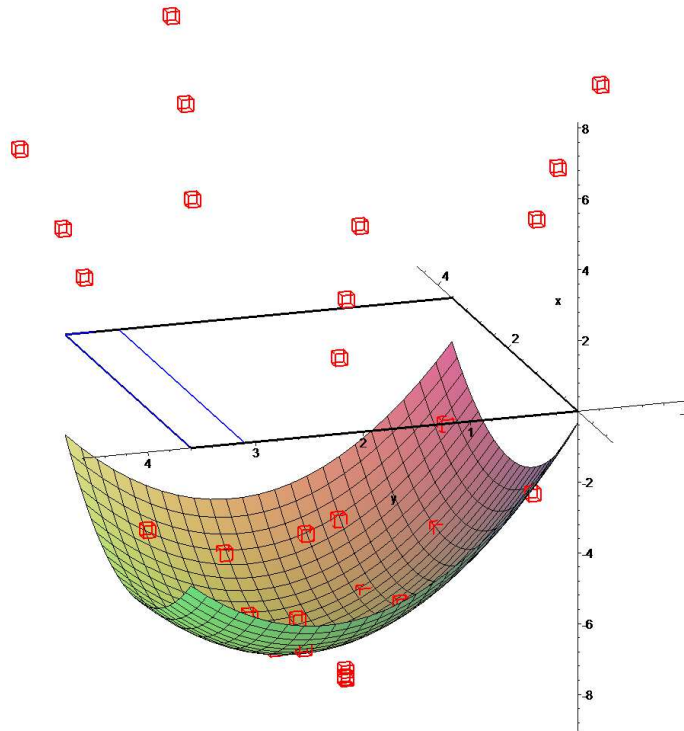


Figure 10 : Surface and sub-surface temperatures at the end of the 3rd cooling stage

Taking account of the measurements at the room surface, interpolation can be applied to the entire surface. The Figure 10 presents such a 3D plot of these values. The blue line represents the floor ventilation box. The lowest measured temperature of salt surface is -7.1°C and the highest is -1.4°C . Clearly the distribution of final temperatures is not uniform over the salt floor and it is strongly influenced by:

- a) heat loss below the walls of the cold room
- b) air flow above the floor, the speed of which is decreasing with the distance to the ventilation box.

This analysis is confirmed by the pictures taken by the thermal camera placed on the room ceiling. Reconstitution of the various images shows the room surface temperature (See example Figure11). We can clearly see on this type of image the influence of the walls and of the distance from the fans.

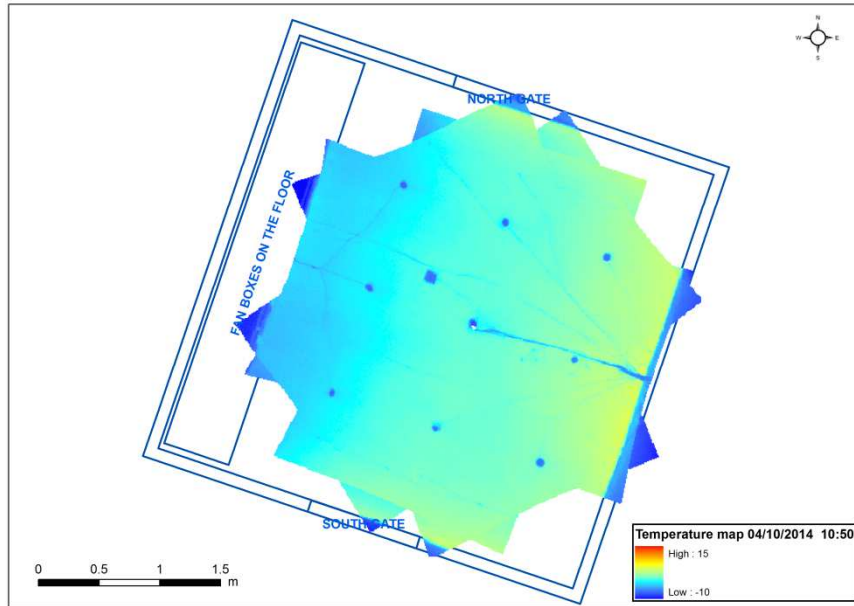


Figure11: First cooling stage - Map of the surface temperature after 1 day of cooling.

3.3 Depth temperature measurements

Temperature measurements are presented according to a vertical axis of between 0 and 80 cm. The measurements were recorded by the sensors placed in the small vertical bore hole at the centre of the room. Sensor T2 placed higher up follows the trend observed previously at the surface, whereas the deepest sensor T5 stabilises at a temperature barely below 0.

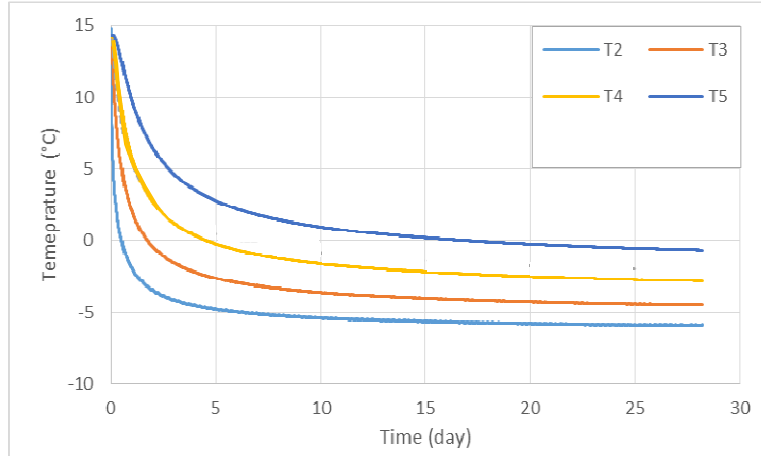


Figure12: Temperatures of Pt100 sensors inside the cooled salt rock mass. The respective depths of Pt100 sensors T2, T3, T4 and T5 into the central bore hole are 4, 24, 44 and 80 cm.

We can also see from the curves that cooling rate is a lot slower deeper down. Therefore over the first few hours, the difference in temperature is relatively high, at around 20°C. It then decreases as the cold penetrates, to reach an almost stable temperature difference of around 5°C.

3.4 Heat flux.

Heat flux is measured in order to look at heat exchange at the room surface (See Figure 13). The flux increases very rapidly when cooling starts as the difference in temperature between the air and the salt is high. The flux then tends to reach a constant value of $60 \text{ W} \cdot \text{m}^{-2} \cdot \text{s}^{-1}$

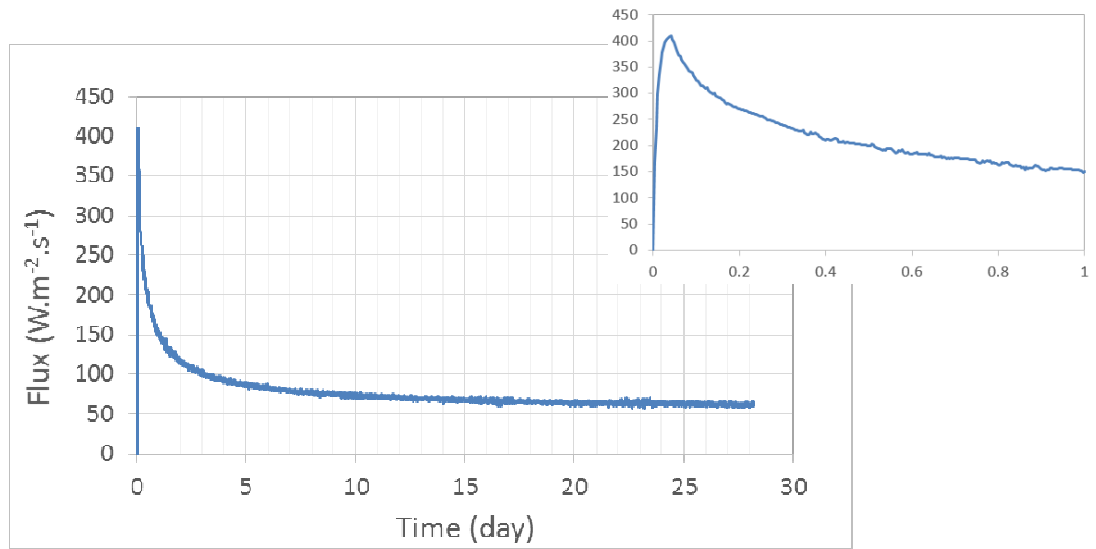


Figure 13 : Heat flux during cooling (and zoom on the first day).

The local value of flux can be used to calculate a value of the heat transfer coefficient. It is equal to the value of heat flux divided by the difference between the salt surface temperature and the air temperature. This was done by using the expression of the air temperature established above and the data of the third cooling stage. The resulting plot (Cf. Figure 14) gives a averaged value of $30 \text{ W.m}^{-2}.\text{C}^{-1}.\text{s}^{-1}$.

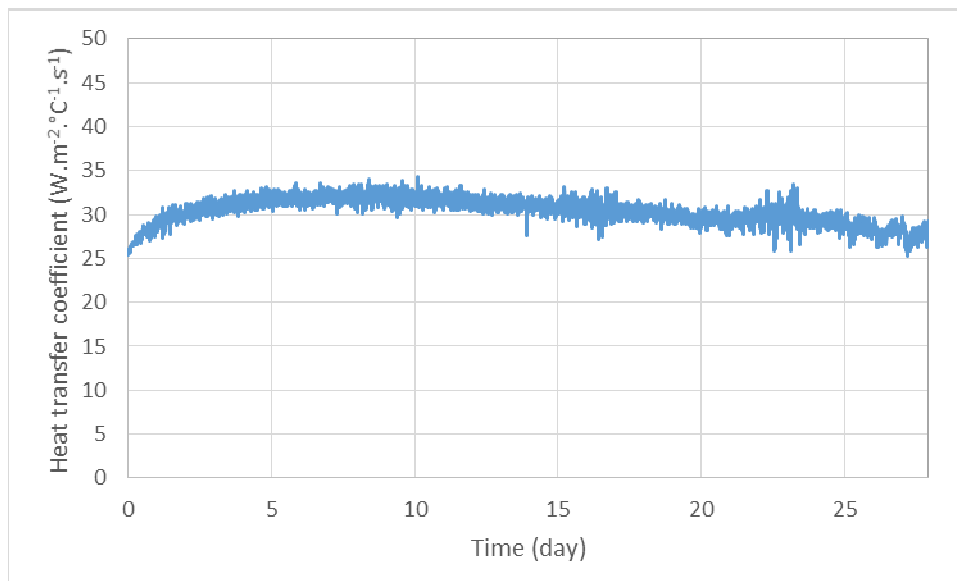


Figure 14 : Local values of the heat transfer coefficient calculated with data of the heat flux sensor

This transfer coefficient will be used for the thermal analysis during the experiment in order to represent the actual thermal stress on the salt formation in a more accurate manner. A full digital model of the temperature in space and time is therefore created and will be used for fine matching with the geomechanical model.

4 Results

4.1 Crack examination

A crack appears from the first hours of cooling (See Figure15).



Figure15: the first crack a few hours after cooling had started

It extends rapidly over more than one metre, perpendicular to the air flow, at around one metre from the fans (See Figure 16), there where the temperature is the coldest. At the end of cooling, the crack aperture was around 0.3 mm.

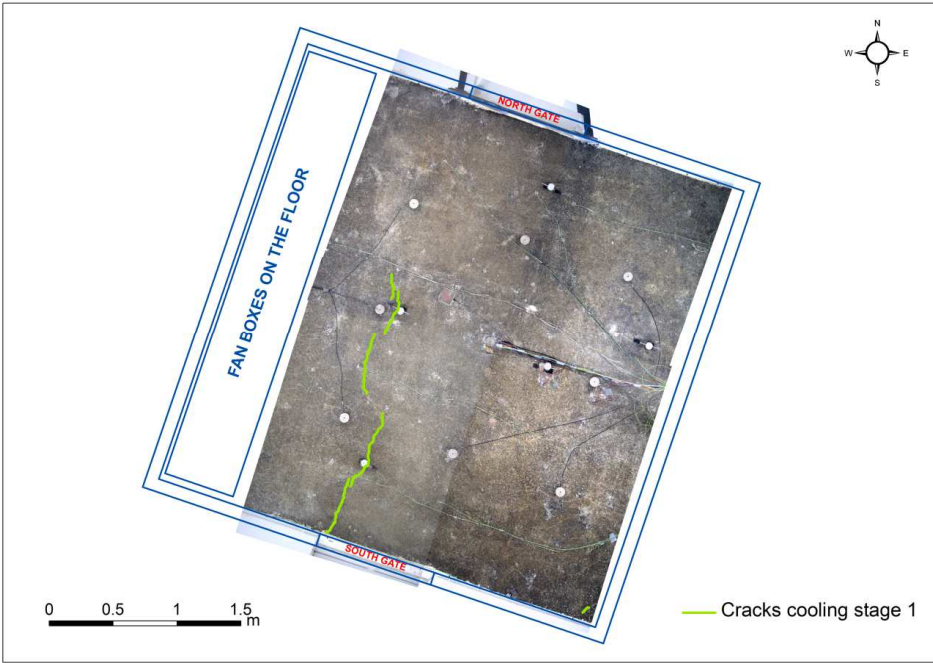


Figure 16 : First cooling stage crack map

On entering the room, we see there is not only a crack, but that the salt surface looks completely "glazed". A myriad of very fine cracks, which do not seem to be very deep, mark the salt surface. It

can be seen when we place a light on the surface, the light does not cross the micro-cracks (See Figure17).



Figure17: Observation of the "glazing" effect of the surface by light transmission.

After initial cooling, a heating cycle was run until the salt temperature returned to almost its baseline state. The crack closed completely and was completely imperceptible to the naked eye.

The cooling-heating cycle was repeated three times. During each cycle, the previously open cracks not only opened again but spread. New cracks also developed and a network appeared to form little by little (See Figure18). Extension of the cracks is nevertheless increasingly reduced during each cycle. The main crack from the first cycle is perpendicular to the air flow at around 1 m from the fans, the crack then spreading to join a second crack, which seems to start parallel with the first, at around 1 m distance from it. At the end of the cooling cycles, maximum crack width measured is 1 mm (See Figure19Figure19).

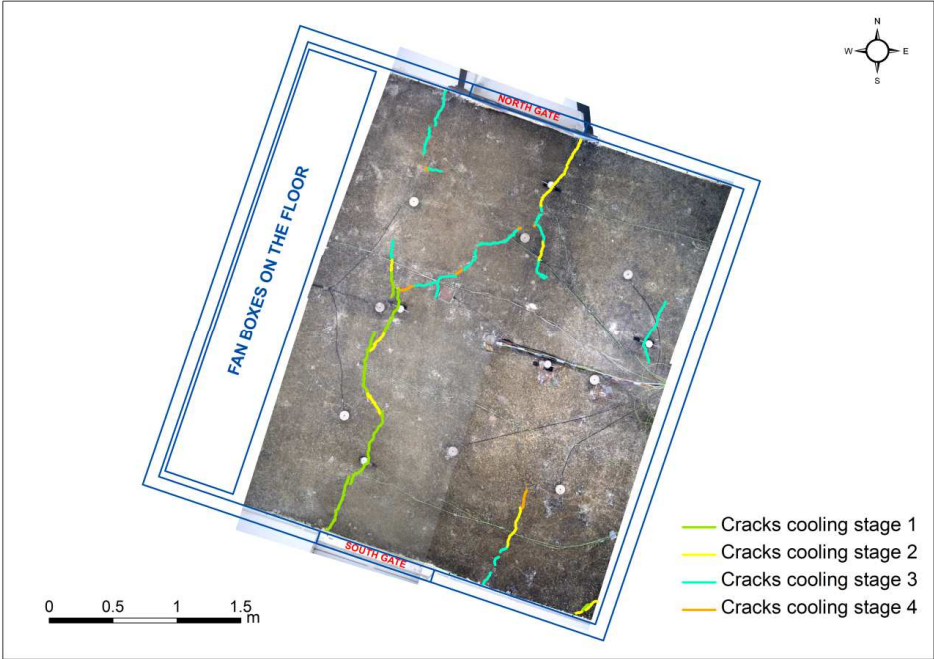


Figure18: Map of cracks reactivated and created during the fourth cooling stage



Figure19: Measurement of the main crack opening at the end of the 3rd cooling cycle using a comparator. The opening is measured at 1 mm after 28 days' cooling.

4.2 Acoustic emissions

From the first cooling phase, the acoustic listening device registered a great deal of events, to such an extent that it was rapidly saturated. It will be necessary to change sensor sensitivity during the experiment to only record the most powerful signals. Figure20 shows the events to be distributed evenly over the entire test area. There were significantly fewer events over the following cycles, then we came back to the initial sensitivity.

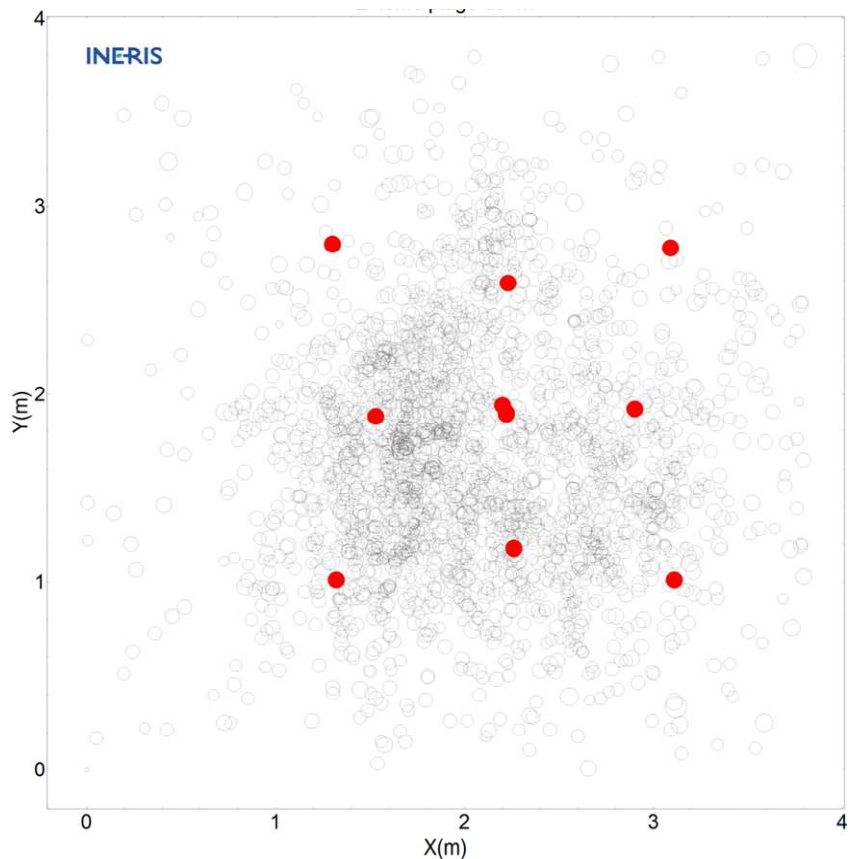


Figure20: Acoustic events during the first two hours of the initial cooling cycle (top view). The red dots show the acoustic sensors at the surface and at a depth. The fans are placed on the left.

Figure21 shows the total number of acoustic events recorded during each cooling cycle. The total number of events is unknown for the first cycle as the system was saturated. By extrapolating the curve recorded over the first few hours (with the same sensitivity as for the following cycles), the number of events is estimated at between 47,000 and 60,000. The first cycle is by far that which produced the most acoustic emissions with 2 to 3 times more events than for the second cycle. The number of events decreases further during the third cycle.

This data is highly consistent with the development of the cracks observed visually during the cycles. In effect, during the first cooling cycle, the first visible crack forms over a distance of more than one metre, but comes with many very fine cracks, forming over the entire surface. For the following cycles, existing cracks opened again (phenomenon generating few emissions) and spread (emission-generating phenomenon). The number of newly formed cracks is also increasingly reduced.

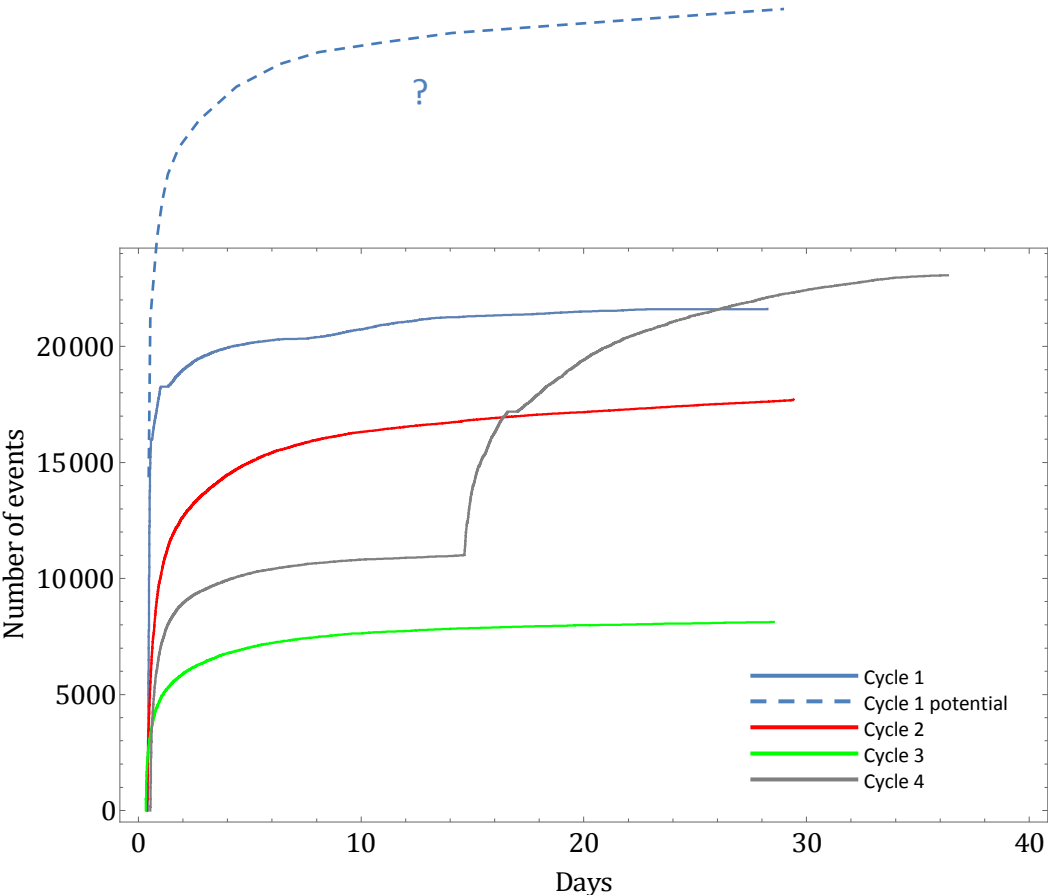


Figure 21: Number of acoustic events recorded by the device during the various cycles. As the system was very rapidly saturated during the first cycle, the sensitivity had to be reduced after a few hours. The dotted curve is a rough estimation of the number of events if the same sensitivity had been maintained for all cycles.

To end the experiment, a fourth cooling cycle was applied. It was divided into two cooling phases: one phase at a temperature of -9°C for 14 days as previously and one phase at -25°C . During the first phase the number of events increased slightly compared to the third cycle, whereas the thermal sollicitation was the same. It remains however fairly low. However, acoustic activity increases significantly during the second phase, with the unprecedented sollicitation. It remains nevertheless significantly lower than the maximum number of events from the first cycle.

No events were detected during the heating phases (closing cracks phases).

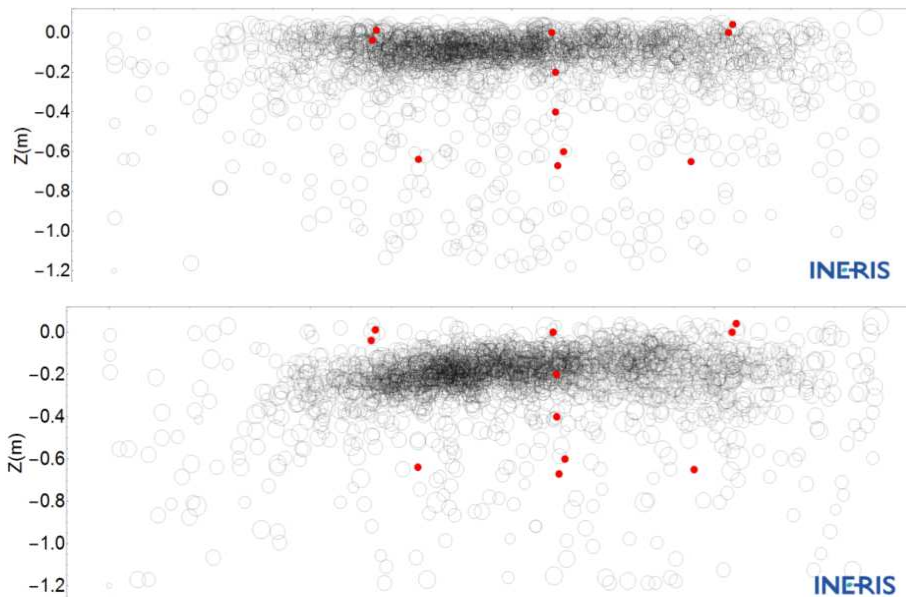


Figure22: Location of acoustic emissions during the first hour (top) then the second hour (bottom) during the first cooling cycle (cross-section view according to the central axis of the room parallel to the air flow). The red dots show the acoustic sensors at the surface and at a depth. The fans are placed on the left.

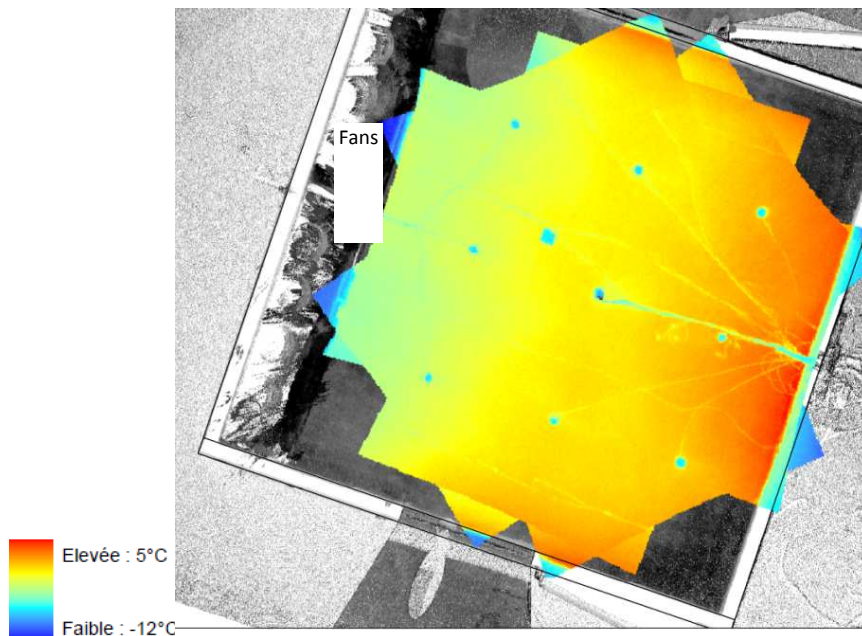


Figure23: Thermal image of the room surface after 24h cooling. We see the difference in the temperature according to the distance from the fans.

During each cycle, the acoustic emissions are initially located at the surface before descending deeper as the salt cools. Figure22 shows a slightly higher concentration of events during the first

hour on the left, nearest to the fans. During the second hour, we see a slight increase in depth on the left side. This is related to the heterogeneity of the temperature at the surface. The air flow coming out of the fans is cold but heats as it moves further away (See Figure23).

The depth of the events over time is shown on Figure24 for the various cycles. The maximum depth reached is around 90 to 100 cm for the first cycle and 80 cm for the following cycles, including for the cycle at -25°C. Maximum cracking depth does not therefore increase with the number of cycles. Contraction of the salt from the cooling is mainly absorbed by reopening of the cracks already formed in the previous cycle, and possibly by the formation of new cracks, but which remain in the same area as for the first cycle. We can conclude that the presence of cracks does not affect cooling of the formation and that they are not therefore a vector propagating the cold with respect to thermal conduction through the salt. This is explained by the fact that the cracks are extremely fine. The quantity of cold air contained in a crack is very small compared to the contact surface represented by the rims of the crack. The temperature of the air in the crack therefore balances very rapidly with the temperature of the surrounding rock, the temperature of which is in turn governed by conduction.

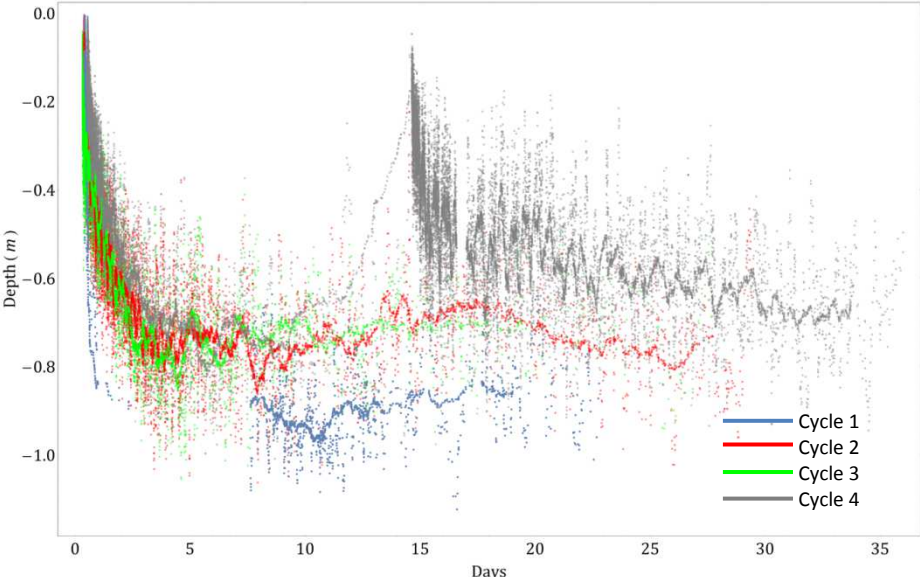


Figure24: Depth of acoustic emission sources over time.

4.3 Post-mortem analysis



Figure25: Post-mortem coring

At the end of the experiment, after removal of the cold room, core samples were taken from the site (See Figure25). K2 core samples were taken from the main crack. On the core sample, we can follow the crack which extends vertically up to around 75-80 cm, depth from which the crack leaves the bore hole (See Figure 26).

This result is highly consistent with, on the one hand, the depths observed with the acoustic emissions, and on the other hand, our theoretical knowledge on cracking related to thermal cooling. The theory provides for the formation of a myriad of very small superficial cracks in the event of thermal shock. Then, as cooling takes place, crack selection seems to emerge and only a few cracks become deeper whilst others close. Penetration depth is believed to be of the same order of magnitude as the distance between the cracks.

The other core samples taken from secondary cracks also show vertical cracks but at a lower penetration depth, of around 30 to 40 cm.

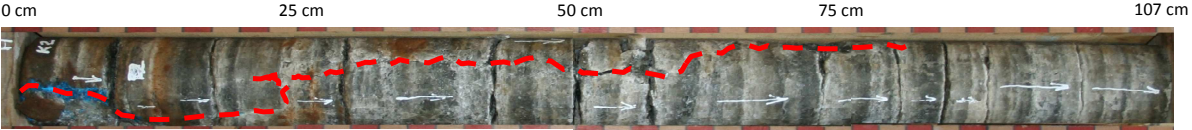


Figure 26 : K2 core sample image reconstruction. The red dotted line shows where the crack was followed.

5 Interpretation

Following this experiment, various digital models were created to interpret the results. They were combined thermomechanical models using the finite element method. Coupling is said to be low as the calculation takes account of the effects of temperature on the mechanics, but the effects of the mechanics on temperature are not taken into account. Therefore heating by friction in the case of this experiment is insignificant.

5.1 IUB/Leibniz Universität Hannover model

The first model was created by IUB using the Flac3D software based on the Finite Element Method. Gridding is three-dimensional, taking the layer of marl located under the salt into account (See Figure27). The experimental site is very finely modelled, including especially the two lateral cuts at the edges of the salt slab.

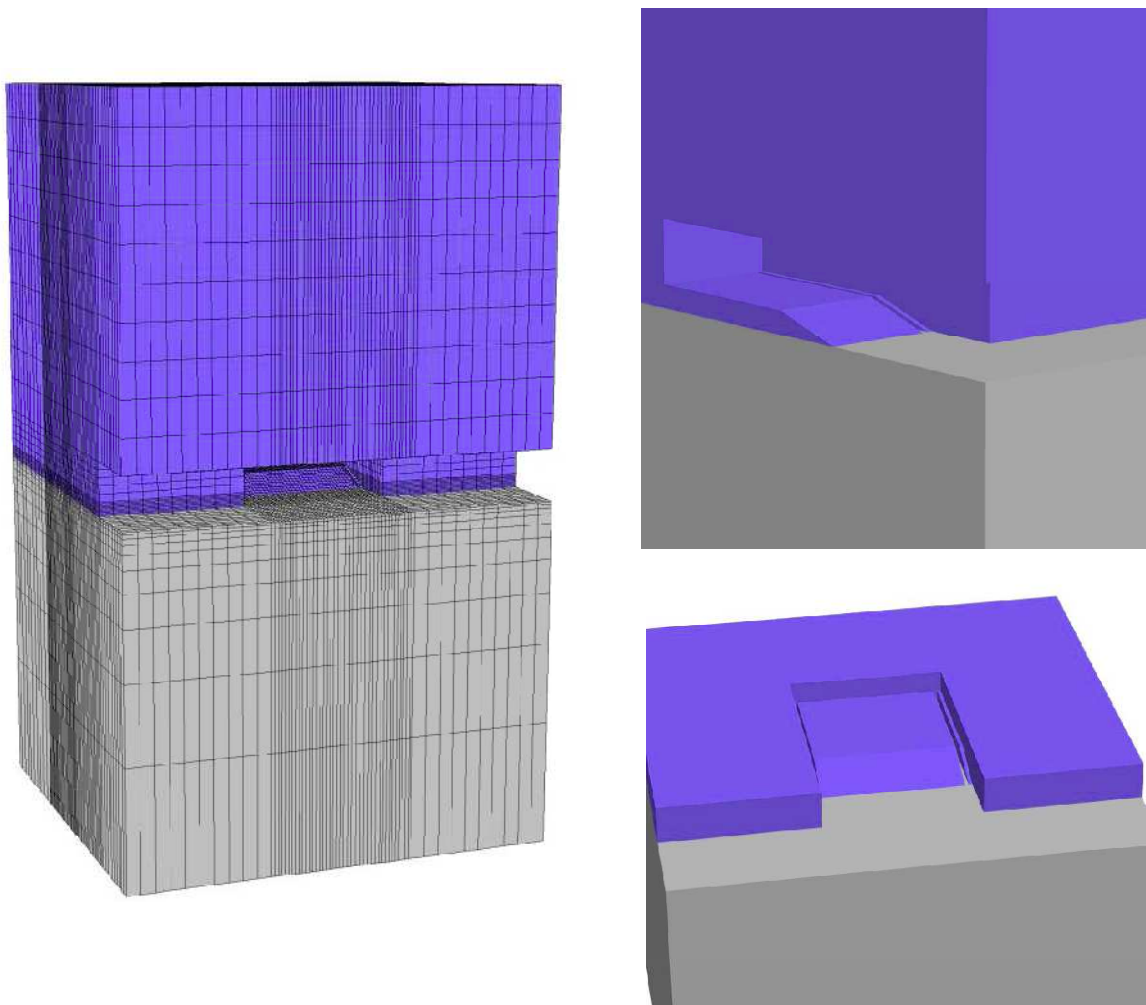


Figure27: Flac3D calculation model global view (left) and close up view with vertical (right up) and horizontal (right down) cross section through the test site. The salt is in blue, the marls in grey.

In this model, thermal stress is applied evenly over the test surface on which the cold room was built. The model is used to calculate the temperature in the salt and mechanical stress state. As it is a model of continuous media mechanics, the cracks are not modelled.

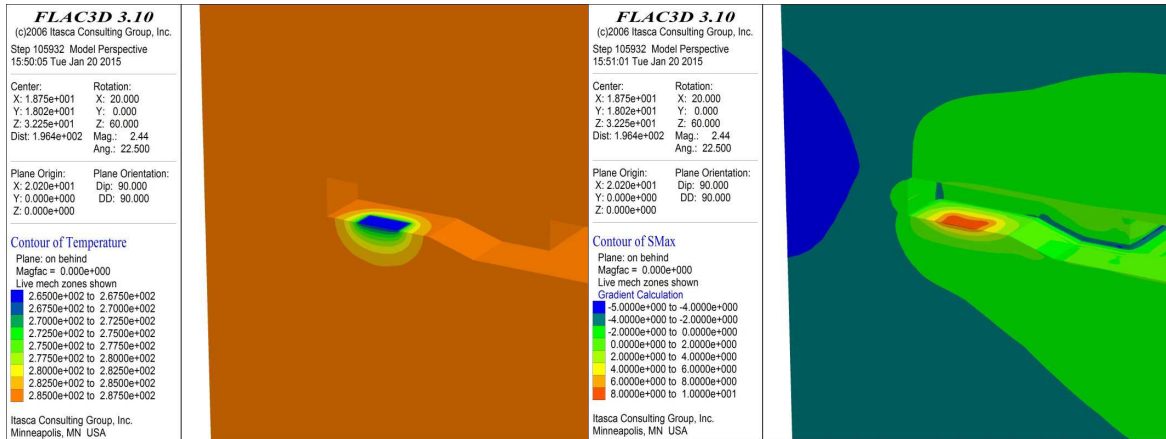


Figure28: Experiment digital model (IUB/Leibniz Universität Hannover). On the left, the temperature in Kelvin, on the right, the principal stress in MPa at the end of the first cooling cycle.

Figure28 shows temperature distribution in the formation and the distribution of the resulting stresses, Figure 29 shows the principal stresses at the salt surface over time.

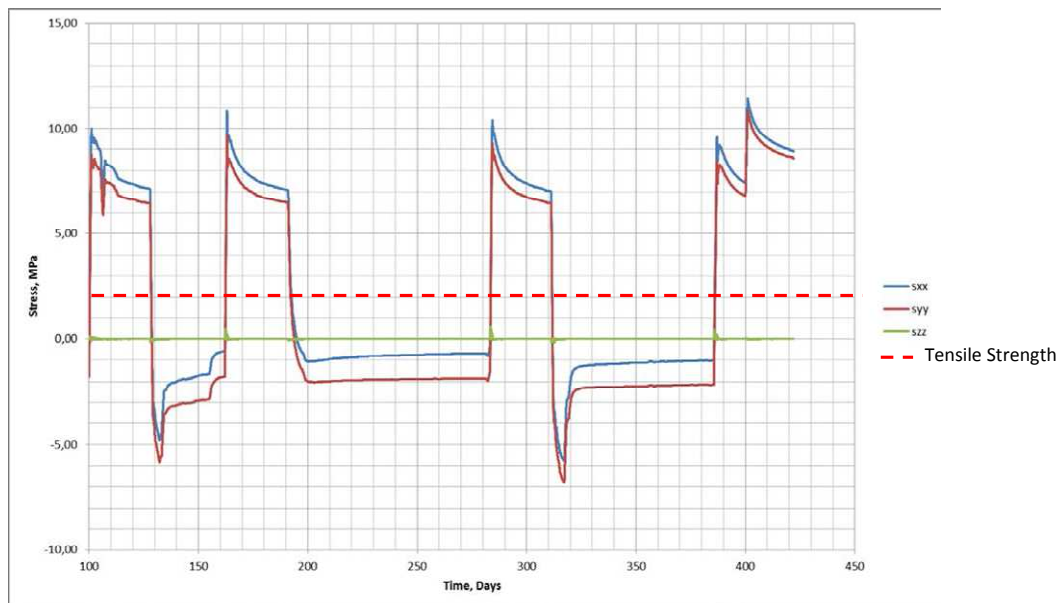


Figure 29 : Stress development over time (ground surface), the red dotted line indicates the tensile strength of the salt.

The principal surface stresses are initially non-existent or very close to zero. They become positive (tensile) and very largely exceed the salt's tensile strength which is around 2 MPa. This model very clearly explains how cracks form at the surface.

The tensile stress decreases with depth. At one metre's depth (See Figure 30Figure 30), it only very slightly exceeds the tensile strength. The curves show the depth of the area under tensile stress which is around one metre, a value consistent with the crack penetration depth observed.

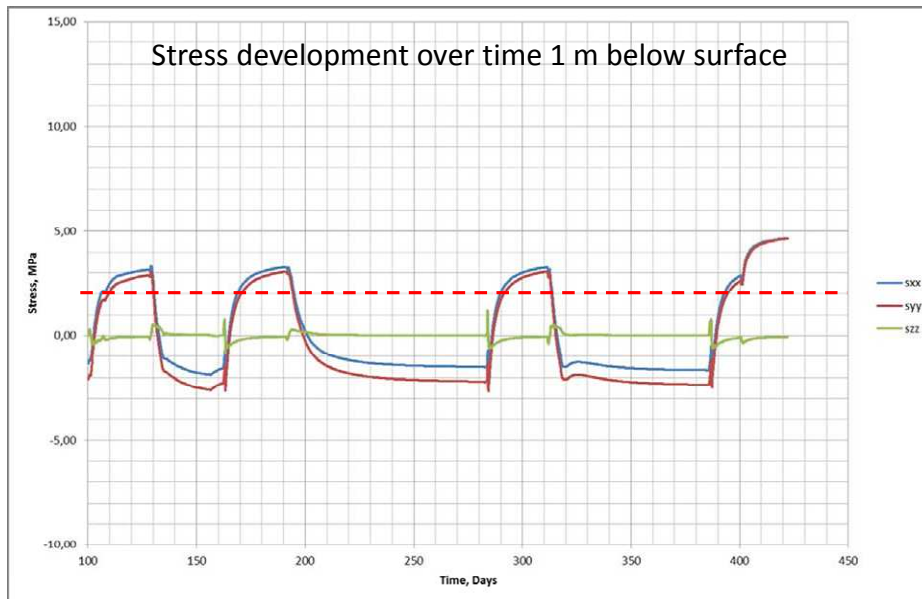


Figure 30 : Stress development over time (1m below ground surface)

5.2 Mines ParisTECH'/ARMINES model

The second model was created using the COMSOL Multiphysics software for the thermal part and the VIPLEF3D software for the mechanical part. As for the previous model, the software is based on the Finite Element Method (See Gridding Figure31).

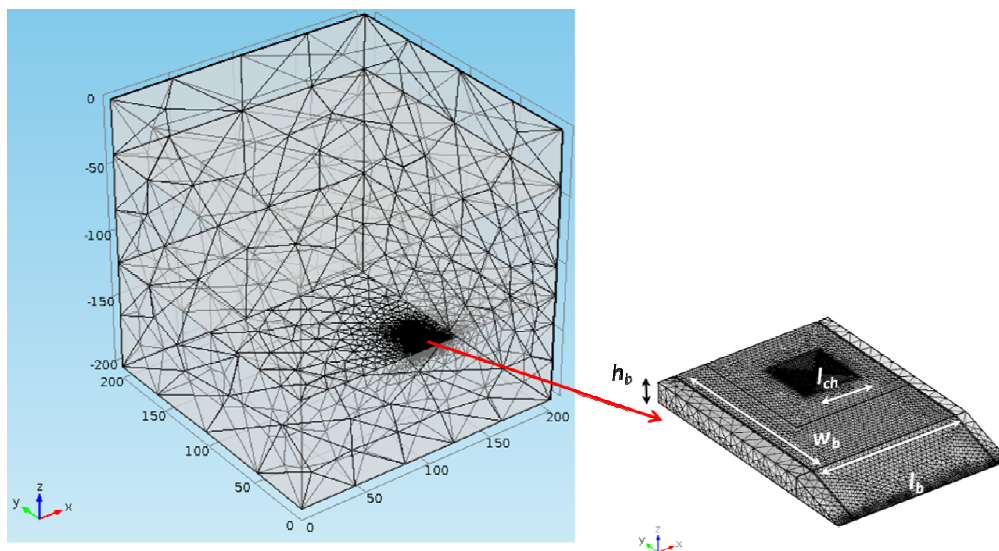


Figure31: Mechanical model gridding

A thermal model was created first to reproduce temperature stress in as fine a manner as possible. The readings showed that the temperature was not homogeneous due to the test conditions. The various model parameters were set to highly accurately reproduce the temperature observed at all points in the formation. As an example, Figure32 shows the comparison between the experimental temperature measurements at different depths and the values from the thermal model. We can see that the curves are perfectly adjusted.

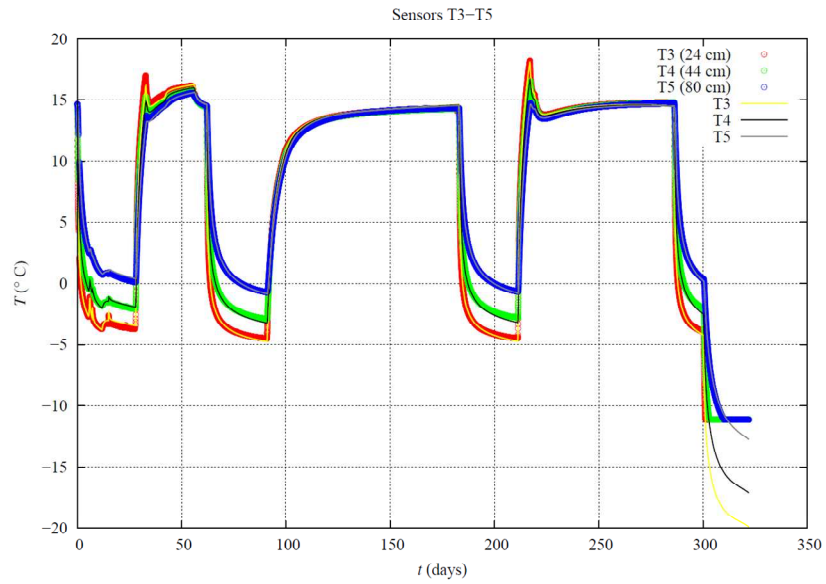


Figure32: Comparison of the temperature recorded (red, green and blue circles) at various depths (24, 44 and 80 cm respectively) and the temperature from the thermal model (yellow, black and grey lines respectively).

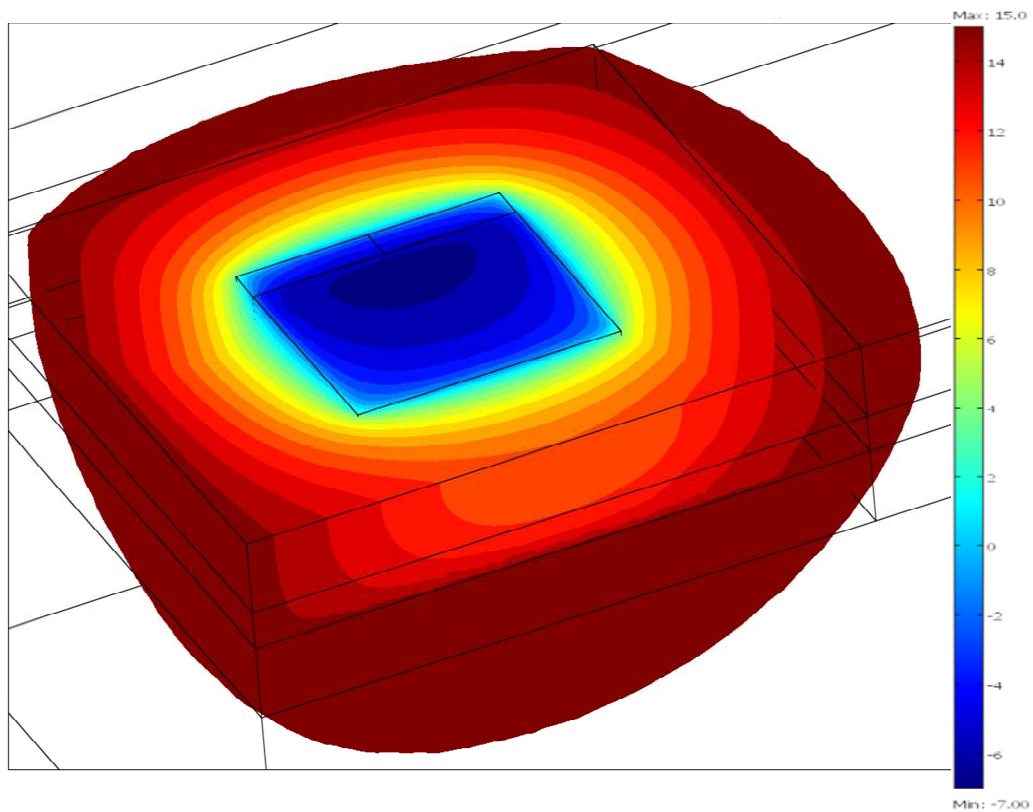


Figure 33 : Heat depth penetration after 28 days 3D view.

This thermal model therefore reproduces the temperature observed at each of the 35 sensors highly accurately and their extrapolation to the entire formation (See Figure 33). It takes the heterogeneity of cooling relating to the experimental conditions into account. On this model we see that the formation is affected by cooling up to around 5m depth (See Figure 34).

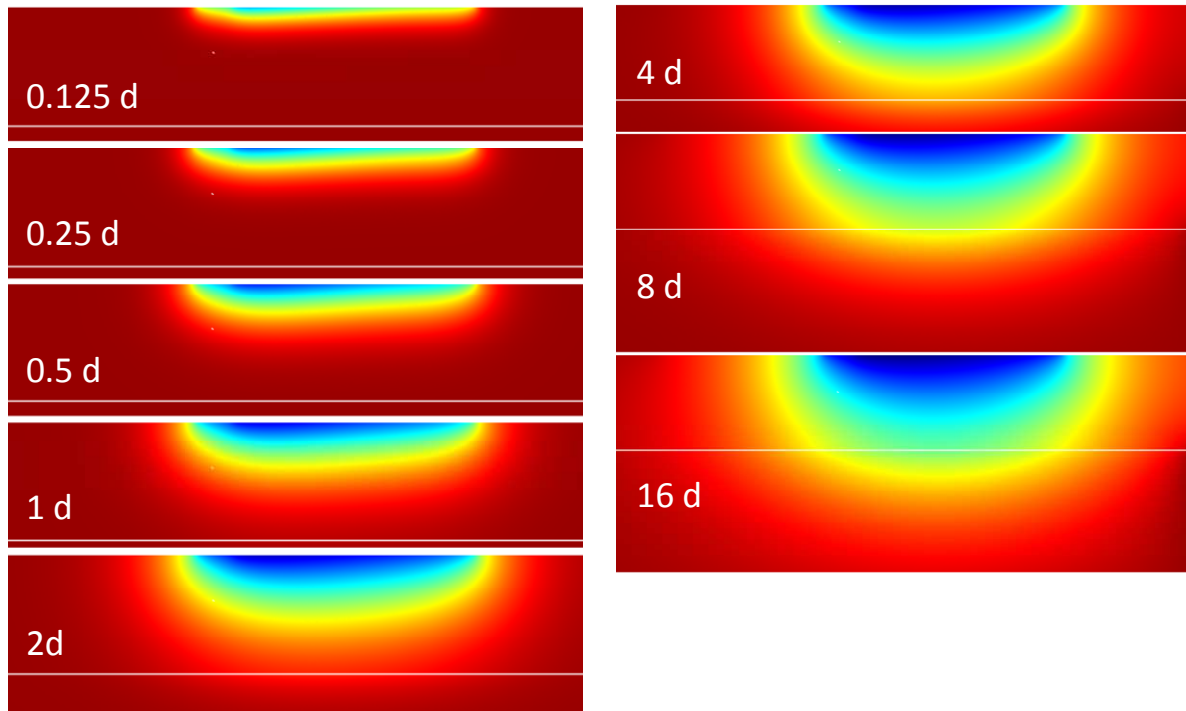


Figure 34 : Vertical cross section of the heat depth penetration at different date.

A mechanical calculation is performed on the basis of this thermal model. It is used to determine the whole stress in the formation . If we look at the room surface (See Figure35), we see there is a strong correlation between temperature and stress: in the coldest area, near the fans, the major principal stress rapidly exceeds the salt's tensile strength which is around 2 MPa, and then reaches its maximum up to 10 MPa. The maximum is of the same order of magnitude as that calculated by the model produced by IUB.

Figure36 shows the major principal stress at different times. We can see the depth of penetration of the tension zone is around a metre. This is consistent with the penetration depth of the cracks identified by the acoustic emissions. We also see that the stress values are at the maximum at the surface at the beginning of cooling, when the temperature difference between the surface and the formation is significant. Stress then decreases slightly as the temperature evens out in the formation. This suggests that it is effectively the temperature difference which causes the greatest stresses and therefore cracking.

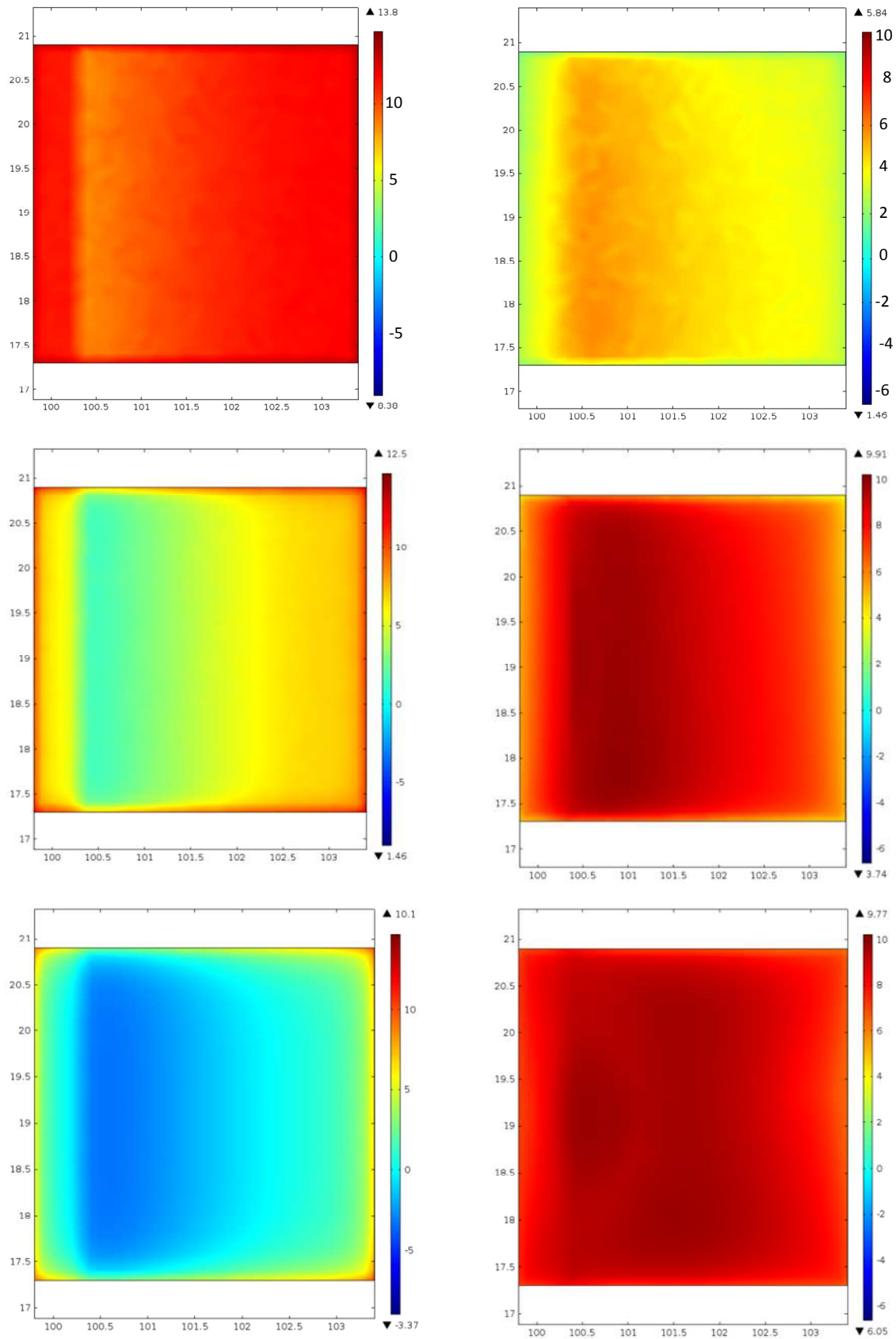


Figure35: Digital model of the room surface after 30min, 2h and 12h cooling (top to bottom). The fans are placed on the left. The temperature is shown in the left-hand column in °C and the major principal stress in the right-hand column in MPa

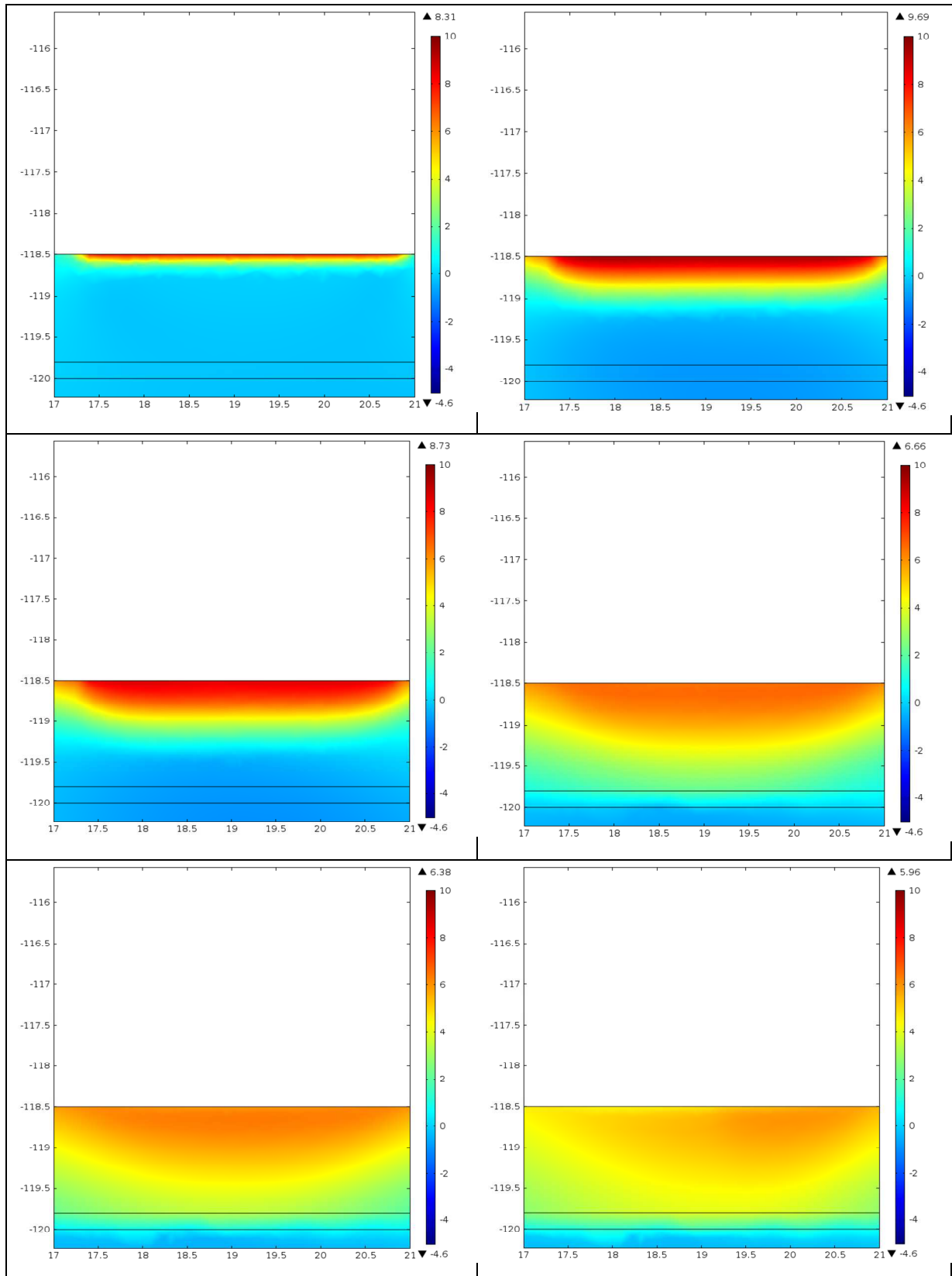


Figure36: Side-on cross-section of the major principal stress (in MPa) 1h, 12h, 1 day, 5 days, 10 days and 20 days after the start of cooling. The fans are placed on the left. We see penetration in the tension zone with high values in the first few hours, when the temperature difference is significant (stress of up to 10 MPa at the surface) and slightly decreasing values as the temperatures even out in the formation. Tensile stress penetration is around one metre.

The additional information brought by this second model concerns stress direction. During initial cooling and from the first hour, we saw the main crack open parallel to the fans, around a metre away from them. If we display the direction of the principal stresses calculated at certain points along the main crack (See Figure37), we see that the highest stress is perpendicular to the crack. Stress direction is therefore highly consistent with mechanism of opening of the crack observed.

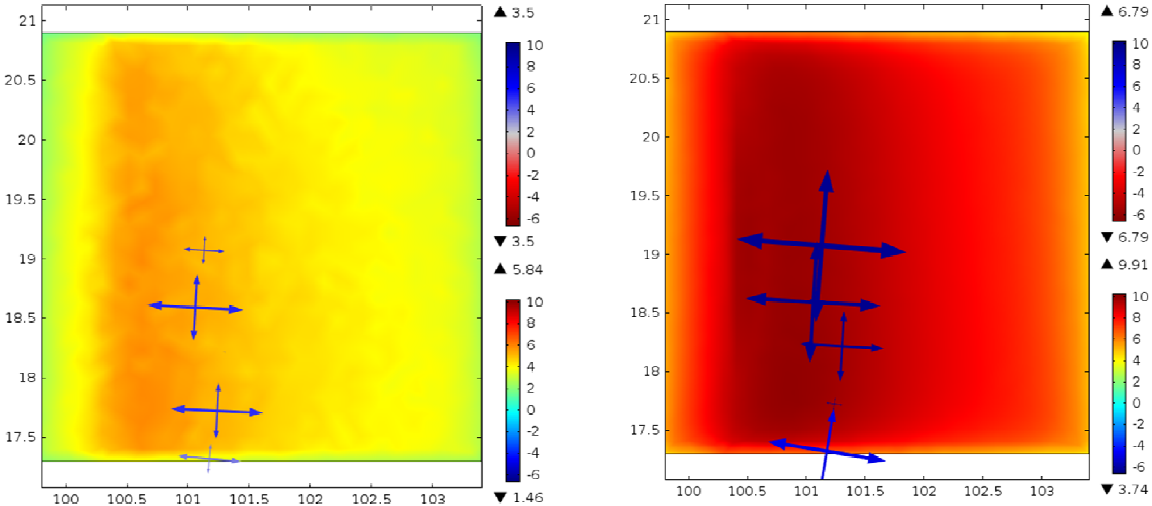


Figure37: Major principal stress at the surface of the room, 30 min and 2h after the start of cooling (Mines ParisTech'). The arrows on the left-hand picture show the direction of the principal stresses at the various points at which the crack was actually seen. We see that the highest stresses are directed perpendicularly to the main crack, which explains the direction of this crack.

We note that at this stage that models of continuous media mechanics cannot be used to represent the crack or to take into account stress redistribution related to it. Just after the crack appears, the model cannot therefore represent the actual stress state. Nevertheless, the place in which tensile stress develops in the model is highly consistent with the actual place in which the crack is observed. Also, the experiment shows that the various cycles do not affect it significantly even for higher temperature variations.

The consistency between the actual cracked areas and the tension zones in the digital continuous models is a significant result as it confirms the relevance of these digital models, which are conventionally used for the proportioning of salt caverns (for designing salt caverns ?). By introducing temperature variations, we will be able to estimate the areas potentially affected by thermal cracking and to evaluate the consequences of it. These tools can be used to refine existing criteria and possibly put forward operational requirements for minimising the effects of the rapid temperature variations.

6 Conclusion

Due to the change of gas storage salt cavern operating procedures (natural gas, air, or even hydrogen etc.) the question of the impact of rapid temperature variation on the salt has become an important question over the last few years.

To provide tangible elements of response, the Solution Mining Research Institute (SMRI) wanted to conduct a full-scale experiment on a salt formation. The primary objective was to verify, via a demonstration, whether a drop in temperature as observed in a gas cavern storage was capable of generating cracks in the cavern walls. If this was the case, the secondary objective was to be able to quantify the phenomenon in order to assess the actual consequences for the storage.

Following the Request For Proposal, an international team was set up to conduct the experiment in the Varangéville salt mine. The team included the Compagnie des Salins du Midi et des Salines de l'Est (CSME - Salins group), the INERIS, Mines ParisTech'/ARMINES, de IUB/Leibniz Universität Hannover and Storengy. The experiment involved the use of a cold room. A salt surface measuring 10 m² was exposed to temperature variation cycles within a 20°C range. The experiment demonstrated cracking caused by rapid cooling of the salt.

The experiment was monitored using a highly comprehensive test system (temperature measurements, acoustic emissions, thermal and digital imaging etc.), such a system cannot be used in an actual salt cavern storage. Crack size, the number of cracks, their direction and the area in which they developed were accurately quantified using this system. The elements were used to confirm the theoretical approach to cracking caused by cold in the salt.

We should note that the experimental conditions can be considered to be extreme compared to the conditions in an actual cavern repository. In effect, the experimental slab is mechanically unloaded before the start of the test. The tensile stresses generated by cooling do not match the compression stresses existing in a salt formation surrounding an actual cavern. Also, the drop in temperature created by the cold room is very rapid compared to the drop in temperature likely to be caused by even very violent withdrawal. Finally, low temperature is maintained for 28 days in the room whereas in an actual cavern, the temperature rises rapidly after withdrawal, via heat exchange in the walls.

Two digital models using the Finite Element Method and reproducing the experimental conditions, were used to calculate the stress state of the salt formation subjected to the temperature variations. The models take the thermal stress in the experiment into account in a highly accurate manner.

Despite the fact that these models of mechanics of heterogeneous media cannot simulate the cracks, we see a strong correlation between distribution of tensile stresses in the salt calculated by the models and the location, direction and maximum depth of penetration of the cracks observed in the experiment.

This consistency confirms the relevance of this type of model for studying cracking phenomena caused by cooling. Extrapolation of these results to actual caverns can be used to study thermal cracking of the salt in the wall of the works and to evaluate the consequences of it. These tools can be used to refine existing criteria and possibly put forward operational requirements for minimising the effects of the rapid temperature drops.

In accordance with the undertaking of the team having conducted the experiment to the SMRI, the experimental data for this project is available to any members of the SMRI wishing to receive it.

7 References

Bauer S., Sobolik S. (2009) - *Pressure cycling in Compressed Air and Natural gas storage in salt: tracking stress states and cavern closure using 3-D Finite Element Code*. SMRI Spring Meeting, Krakow, Poland, 129.

Bérest P., Djizanne H., Brouard B., Hévin G. (2012) – *Rapid depressurizations: can they lead to irreversible damage?* SMRI Fall Meeting, Regina, 64-83.

Brouard B., Frangi A., Bérest P. (2011) – *Mechanical stability of a cavern submitted to high-frequency cycles*. SMRI Spring Meeting, Galveston, Texas, 99-116.

Minkley W., Lindert A., Brückner D. (2011) – *The improved IfG gas storage cavern design concept*. SMRI Fall Meeting, York, UK, 206-217.

Pellizzaro C., Bergeret G., Leadbetter A., Charnavel Y. (2011) – *Thermomechanical behavior of Stublach Gas Storage Caverns*. SMRI Fall Meeting, York, UK, 161-178.

Zapf D., Staudtmeister K., Rokahr R.B. (2012) – *Analysis of thermal induced fractures in salt*. SMRI Spring Meeting, Regina, Saskatchewan, 47-62.